

Vertical Pillar-Superlattice Array and Graphene Hybrid Light Emitting Diodes

Jung Min Lee,[†] Jae Woong Choung,[†] Jaeseok Yi,[†] Dong Hyun Lee,[†] Monica Samal,[§] Dong Kee Yi,[§] Chul-Ho Lee,^{||,⊥} Gyu-Chul Yi,[⊥] Ungyu Paik,^{*,†} John A. Rogers,^{*,#} and Won Il Park^{*,†}

[†]Division of Materials Science and Engineering, [‡]Department of Energy Engineering, Hanyang University, Seoul 133-791, Korea, [§]Division of Bionanotechnology, Kyungwon University, Sunnam city 461-831, Korea, ^{||}Department of Materials Science and Engineering, Pohang University of Science and Technology (POSTECH), Pohang 790-784, Korea, [⊥]National Creative Research Initiative Center for Semiconductor Nanorods and Department of Physics and Astronomy, Seoul National University, Seoul 151-747, Korea, and [#]Department of Materials Science and Engineering, University of Illinois at Urbana–Champaign, Urbana, Illinois 61801

ABSTRACT We report a type of device that combines vertical arrays of one-dimensional (1D) pillar-superlattice (PSL) structures with 2D graphene sheets to yield a class of light emitting diode (LED) with interesting mechanical, optical, and electrical characteristics. In this application, graphene sheets coated with very thin metal layers exhibit good mechanical and electrical properties and an ability to mount, in a freely suspended configuration, on the PSL arrays as a top window electrode. Optical characterization demonstrates that graphene exhibits excellent optical transparency even after deposition of the thin metal films. Thermal annealing of the graphene/metal (Gr/M) contact to the GaAs decreases the contact resistance, to provide enhanced carrier injection. The resulting PSL-Gr/M LEDs exhibit bright light emission over large areas. The result suggests the utility of graphene-based materials as electrodes in devices with unusual, nonplanar 3D architectures.

KEYWORDS Pillar array, graphene, light-emitting diodes, 3D architectures, transparent electrodes

Vertical arrays of one-dimensional (1D) semiconductor crystals, such as nanowires^{1–4} and pillars,^{5,6} are of interest partly because of their promise for application in advanced optoelectronics and photovoltaics. Compared with planar structures, vertical pillar arrays provide enhanced light extraction in light emitting diodes (LEDs) and light absorption in solar cells, due to the suppressed reflection at the output/input surfaces, increased areas of these surfaces, and photonic crystal effect.^{4,5,7–9} In addition, small heterointerfacial areas in the 1D pillar structures can effectively relieve strain in way that has the potential to prevent adverse effects of large lattice mismatches.¹⁰ Several recent attempts have been made to improve the device performance by exploiting these advantages.^{5,6} Layouts that involve air gaps between the pillars offer enhanced ability to accommodate flexural (bending) deformation without fracture,^{11,12} thereby providing advantages over those achievable by making the devices thin and placing them near the neutral mechanical plane.¹³ These collective mechanical and optical characteristics are of interest for various classes of optoelectronic device. Practical use of 1D structures in device applications generally requires, however, the formation of window electrodes on the top surfaces for current injection. The established approach to the formation of such electrodes

involves filling the gaps between the pillars with other materials, such as polymers or spin-on glass, and coated with conducting layers.^{1,6,12,14} These materials affect the thermal, optical, mechanical, and electrical properties in ways that might not be desirable for certain modes of use (e.g., they reduce the degree of bendability in mechanically flexible devices).

Here, we describe a new strategy that combines air-gap 1D pillar superlattice (PSL) arrays with 2D graphene sheets as top electrodes to produce an unusual type of LED, where the graphene mounts directly on the PSL to form a freely suspended structure. In this approach, graphene sheets provide efficient current spreading and injection into the active regions of the PSL for light emission, with minimal optical absorption or reflection. These results suggest, more generally, the potential for use of graphene-based materials as electrodes for nonplanar or 3D optoelectronic and photovoltaic devices.

Graphene sheets, compared to transparent conducting oxides (TCOs), possess additional attractive features, such as unusually large mechanical strength and elasticity.^{14,15} Free-standing graphene sheets can be readily obtained by several methods and techniques for transfer onto arbitrary substrates now exist.^{11,15,17,18} These developments, combined with the attractive intrinsic characteristics of the materials, create opportunities to use graphene in exceptional circumstances where TCOs are not suitable due to their brittleness, their requirement for direct deposition in

* Corresponding author. E-mail: wipark@hanyang.ac.kr (W.I.P.); upaik@hanyang.ac.kr (U.P.); jrogers@uiuc.edu (J.A.R.).

Received for review: 02/23/2010

Published on Web: 07/07/2010



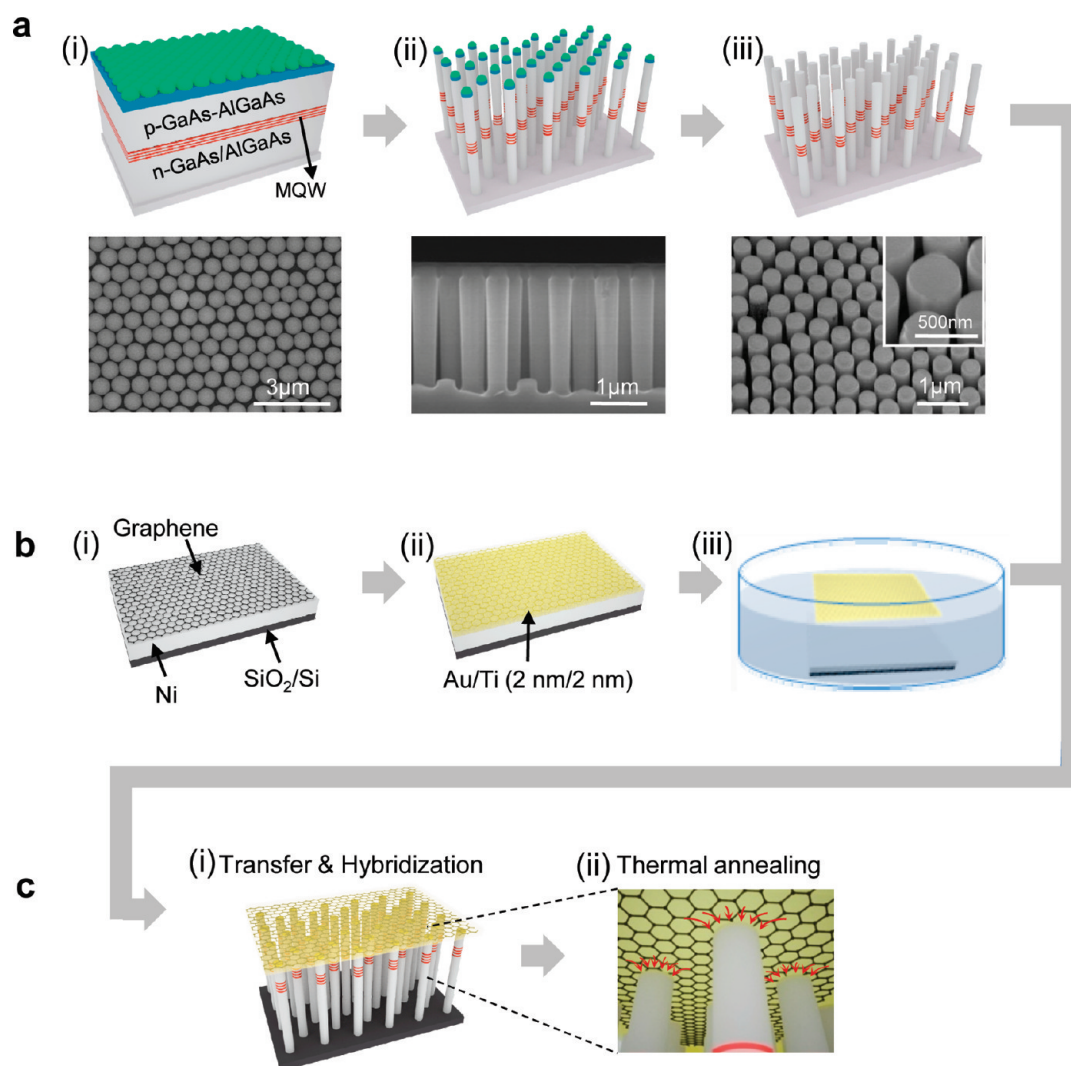


FIGURE 1. Schematic illustration of the key steps for fabricating PSL-Gr/M architectures. (a) Steps for fabricating vertical PSLs arrays: (i) self-assembly of silica spheres on PMMA-coated semiconductor epilayers, (ii) ICP etching to produce the PSL array, and (iii) removal of silica spheres and PMMA layers with sonication in acetone. SEM images of the samples at each step appear at the bottom. (b) Steps for fabricating free-standing sheets of Gr/M: (i) graphene synthesis, (ii) metal layer deposition, and (iii) separation of the Gr/M sheet from the substrate. (c) Integration of the PSL array and Gr/M followed by thermal annealing.

vacuum and often at high temperatures, and their difficulty in coupling to nonplanar 3D device platforms. To exploit graphene in such applications, it is essential to control the electrical contact properties. In PSL array and graphene hybrid LEDs, direct contact of graphene to the inorganic semiconductors generally leads to high injection barriers that degrade performance and frustrate reliable operation. One strategy to overcome this limitation involves exploiting graphene as a deposition site for metal atoms; the graphene in this case provides diffusion pathways to the pillar tips,¹⁹ where interfacial reactions lead to improved contact properties for appropriate metals.

Figure 1 schematically illustrates the steps for fabricating the devices. First, a vertical array of PSL structures was fabricated from group III–V epitaxial semiconductor layers by combining colloidal nanosphere assembly and deep inductively coupled plasma (ICP) etching techniques

(Figure 1a). The epitaxial semiconductor layers include $\text{Al}_{0.25}\text{In}_{0.5}\text{Ga}_{0.25}\text{P}/\text{Ga}_{0.6}\text{In}_{0.4}\text{P}$ (6 nm/6 nm) multi-quantum well (MQW) structures sandwiched in p-type contact-spreader-cladding layers ($\text{GaAs}-\text{Al}_{0.45}\text{Ga}_{0.55}\text{As}-\text{Al}_{0.6}\text{Ga}_{0.4}\text{As}$, 50–800–30 nm) and n-type cladding-spreader-contact layers ($\text{Al}_{0.6}\text{Ga}_{0.4}\text{As}-\text{Al}_{0.45}\text{Ga}_{0.55}\text{As}-\text{GaAs}$, 30–500–500 nm) grown on GaAs substrates. The semiconductor epilayers were spin-coated with poly(methyl methacrylate) (PMMA) and exposed to an oxygen plasma to transform the hydrophobic surface of PMMA into a hydrophilic surface. On the PMMA-coated epilayers, hexagonally close-packed monolayers of silica spheres were deposited by a convective force-driven self-assembly process (Figure 1a-i).²⁰ The samples were heated at 180 °C for 90 s to sink the silica spheres in the PMMA layers, and then exposed to reactive ion etching with CF_4 to reduce the sizes of the silica spheres. By using the silica sphere array embedded in PMMA as an etching

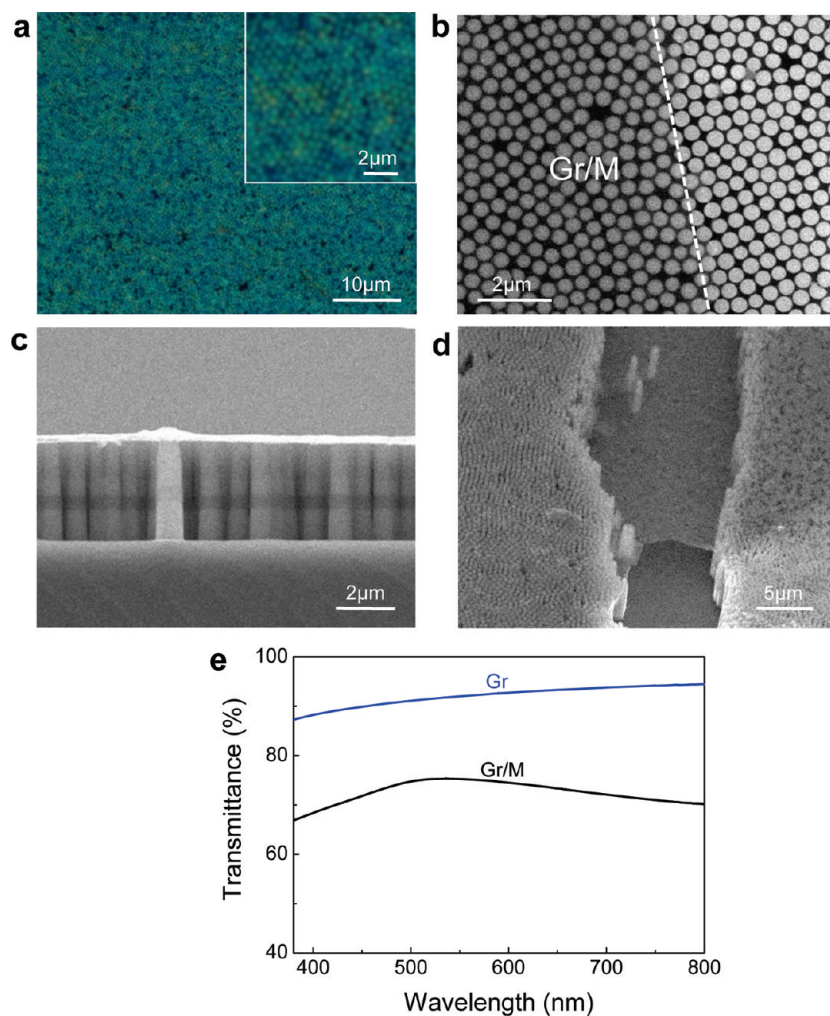


FIGURE 2. (a) Optical images of the PSL-Gr/M architectures. (b–d) SEM images of the PSL-Gr/M architectures. The (b) top view, (c) cross-sectional view, and (d) angle view images show Gr/M sheets suspended over a large areas with the support only of the vertically aligned PSL arrays. The dashed line in (b) shows the boundary of a Gr/M sheets. (e) Optical transmittance spectra of Gr and Gr/M sheets on glass substrates.

mask, ICP etching in BCl_3/Cl_2 plasma produced the PSL array structures (Figure 1a-ii). Etching for 90 s led to vertically aligned cylindrical PSLs with heights of $2\ \mu\text{m}$, average diameters of 400 nm, with smooth sidewalls (bottom of Figure 1a-ii). The silica spheres and PMMA layers remaining at the tips of pillars were removed by sonication in an acetone solution (Figure 1a-iii). The detailed procedures for fabricating vertical PSL arrays appear in the Supporting Information (SI).

Centimeter-scale sheets of graphene were grown on Ni-coated SiO_2/Si substrates by chemical vapor deposition (CVD), using methane (CH_4) as a carbon source under a H_2 and Ar atmosphere at $1000\ \text{°C}$ (Figure 1b-i).¹¹ The low sheet resistance (in the range of $\sim 200\text{--}1000\ \Omega/\text{square}$) and high current carrying capability of the resulting graphene were confirmed by current–voltage (I – V) measurements. Next, thin layers of Ti (below 2 nm) and Au (below 2 nm) were deposited onto the graphene via metal evaporation (Figure 1b-ii). The graphene/metal (Gr/M) sheets were then detached

from the substrates by etching the underlying SiO_2 and Ni layers (Figure 1b-iii). The freestanding Gr/M sheets were floated on an aqueous solution and then mounted on the pillar arrays (Figure 1c-i). Finally, thermal annealing processes were used to improve the electrical contacts (Figure 1c-ii).

Figure 2 shows suspended Gr/M sheets over a large area of vertically aligned PSL arrays. The cross-sectional scanning electron microscope (SEM) image reveals that the Gr/M sheets contact only the tips of the pillars (Figure 2c) and remain tightly suspended over lengths of $\sim 5\text{--}7\ \mu\text{m}$ wide (Figure 2d), demonstrating the robust mechanical properties for this application.

It is noteworthy that both visible light and electron beams can penetrate the very thin layers of Gr/M; thus, the underlying pillars are clearly observed through the graphene sheets in the optical and SEM images (Figure 2a and b). To quantify the optical properties, Gr/M sheets were transferred onto a glass substrate, and the optical transmittance was compared

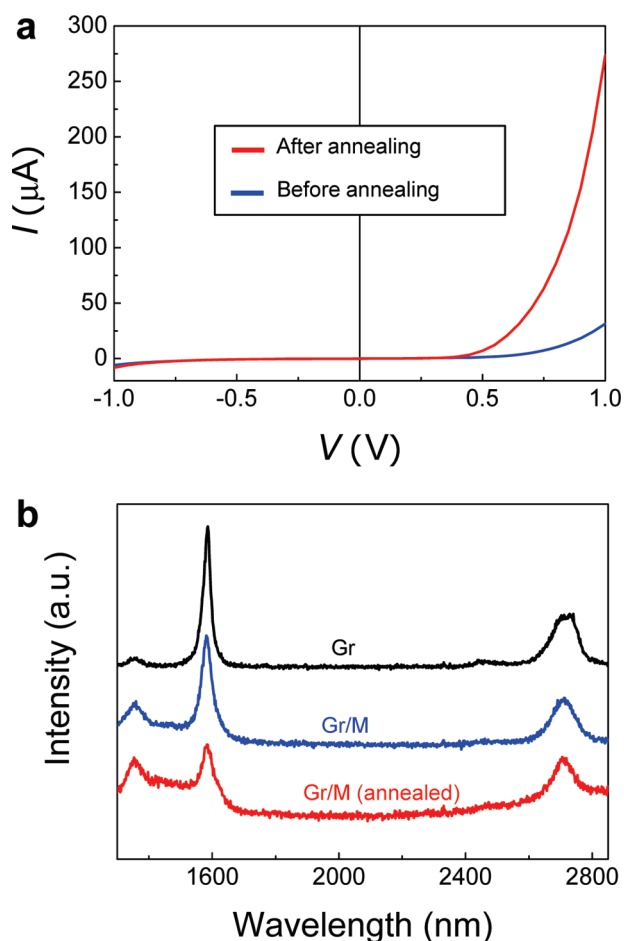


FIGURE 3. (a) I – V characteristic curves of a PSL-Gr/M device (0.3 mm in length and 0.5 mm in lateral width) before and after thermal annealing. (b) Representative Raman spectra of bare graphene (black) and Gr/M sheets transferred onto Si substrates before (blue) and after (red) thermal annealing (excitation wavelength of 514 nm).

to that of a bare graphene sheet. As shown in Figure 2e, bare graphene sheet showed transmittances of $\sim 90\%$ between 400–900 nm, corresponding to an average number of graphene layer below 4–5 (see also Figure S1). Compared with graphene sheet, the Gr/M sheet exhibited a transmittance only $\sim 20\%$ lower, thereby suggesting its possibility for use as a transparent window electrode in optoelectronic and photovoltaic devices.

The current versus voltage (I – V) characteristics of the PSL-Gr/M devices as a function of thermal annealing were also investigated. As shown in Figure 3a, thermal annealing of the device at 340 °C for 20 min resulted in a ~ 9 -fold increase in the forward bias current with no noticeable change in the reverse bias leakage current, thereby enhancing the rectifying behaviors with a forward bias (1 V) to reverse bias (–1 V) current ratio of ~ 35 . The reverse bias leakage current ($\sim 8 \mu\text{A}$) may result from the surface states of the pillar or interface states with its native oxide, both of which may be eliminated with appropriate surface treatments.²² Previous studies of metal ohmic contact to p-GaAs

have shown that thermal annealing activates the interlayer diffusion of Ti to p-GaAs, and that the resulting interfacial reaction lowers the Schottky barrier height and reduces the contact resistance.²³ In our structures, a continuous graphene sheet consisting of a single or a few graphitic carbon networks can provide efficient diffusion pathways for metal atoms. Low activation energies in the range of 0.14–0.8 eV for diffusion of metal adatoms within the plane of graphene sheets have been both theoretically and experimentally confirmed,^{19,24,25} demonstrating that metal atoms are already highly mobile even at relatively low temperatures. Although interplane diffusion is likely less favorable than in-plane diffusion, the extremely thin graphene can enable the stepwise migration of metal atoms from the top graphene sheets to p-GaAs at a higher annealing temperature.²⁵ Therefore, the improved I – V behavior of the PSL-Gr/M hybrid device, especially the increased forward bias current, can be tentatively attributed to the lowering of the Schottky barrier arising from the thermal annealing-induced diffusion of metal atoms to p-GaAs layers and their interfacial reactions. This possibility was further clarified by investigating the contact resistance of Gr/M on a p-GaAs epitaxial layer (planar structures) as a function of thermal annealing (Figure S3). The contact resistance in this case also decreased considerably from $\sim 17\,000$ to $\sim 320 \Omega$ with thermal annealing, in accordance with the increasing forward current of the PSL-Gr/M devices.

The incorporation of foreign elements into graphene sheets may lead to the deformation of the intrinsic structure of the honeycomb crystal lattice. Thus, the structural characteristics of the graphene sheets coated with metal and thermally annealed were characterized by Raman spectroscopy (an excitation wavelength of 514 nm). Because photoluminescence from the underlying pillar structures makes it difficult to probe the Raman signal directly on the devices, we used Si substrates for these measurements. Figure 3b shows the Raman spectra of the bare graphene (black line) and metal-deposited graphene sheets before (blue line) and after (red line) thermal annealing. Similar to the bare graphene, Gr/M sheets, regardless of thermal annealing, exhibited distinct G peaks at 1580–1584 cm^{-1} and 2D band peaks at 2711–2713 cm^{-1} .²⁶ These results, in combination with a G to 2D band intensity ratio in the range of 1.5–2, demonstrate that the graphene sheets remained stable after metal deposition and subsequent thermal annealing.²⁶ Only the disorder-induced D band (~ 1350 – 1355cm^{-1}), which has been frequently observed in sp²-bonded carbon-based materials,²⁷ slightly increased after metal deposition. Previous studies have revealed that the intensity of the D band is related to the basal plane disorder²⁷ and thus, the increased D band in the Gr/M sheets may represent disorders or defects caused by the metal atoms incorporated in the graphene sheets. However, it is noteworthy that the relative D band intensities of the Gr/M sheets are still comparable to

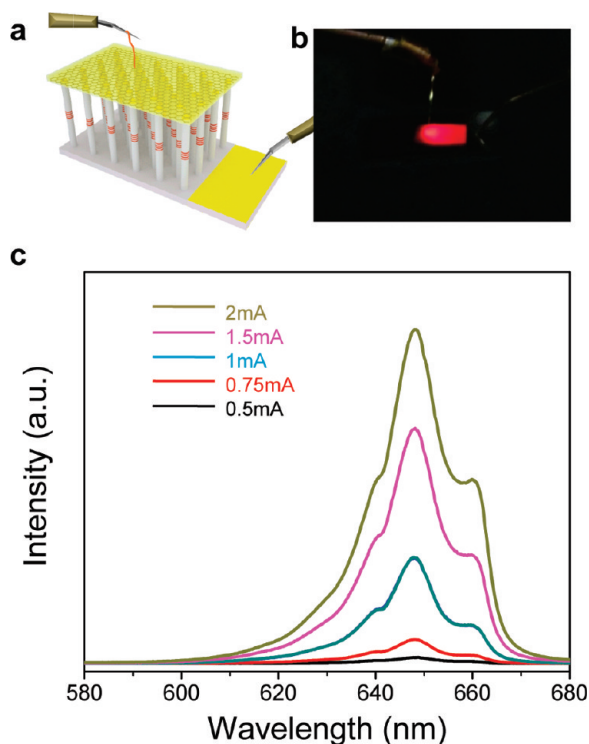


FIGURE 4. (a) Schematic illustration and (b) a photograph of the light emission from PSL-Gr/M LEDs. (c) Room temperature EL spectra of PSL-Gr/M LEDs recorded at various currents.

or even lower than those of graphene sheets prepared by CVD²⁸ or soft chemical synthesis routes.^{29,30}

Figure 4a and b shows a schematic illustration and a photograph of the PSL-Gr/M devices, respectively. The bright electroluminescence (EL) under forward bias is evident. Although electrical contact with the Gr/M window layer was made by using a ~ 0.3 mm thick Au wire attached to a probe tip, bright red light emission was observed from a considerable area ($\sim 0.5 \times 0.3$ cm), where the graphene sheet contacted the PSL array. This observation indicates that the current was effectively spread over the suspending Gr/M window layer. The EL spectra recorded from the forward-biased PSL-Gr/M hybrid LEDs exhibit a dominant emission peak at 648 nm and small shoulder peaks at 638 and 660 nm (Figure 4c), which are tentatively attributed to injected electrons and hole recombination in the GaInP wells in the PSLs. Compared to planar LED mesas,³¹ the forward bias current density of these PSL-Gr/M hybrid LEDs is relatively low, below 10 mA/cm^2 at 3 V. We suspect that the large density of the surface states associated with the ICP etching step contributes to reduced current. Established passivation procedures may eliminate these effects.²² Also, substantial contact resistance between the Gr/M and the p-GaAs remains, even after annealing. More sophisticated ohmic metallization schemes can lead to improvements. The graphene itself exhibits substantial resistance, thereby resulting in a gradual decrease in the light emission intensity as the distance from the Au wire increased. The electrical

property of graphene itself can also be improved with growth techniques that allow large-area, single crystal material with well controlled numbers of layers and low defect densities to meet the conductivity levels required for specific applications while maintaining optical transparency.³²

In conclusion, we demonstrated a type of LED that combines free-standing 2D graphene sheets as top window electrodes with vertical arrays of 1D PSLs. To improve the contact properties of the graphene, we used ultrathin coatings of metals. The key features of the resulting Gr/M sheets include their exceptional mechanical properties and extremely thin nature. These properties enable suspended Gr/M electrodes over large areas with support only from the PSLs, and excellent optical transparency. Thermal annealing-induced diffusion of metal atoms from the top graphene layers to the p-GaAs contact layers improved the electrical contact properties and, thus, enhanced the carrier injection to the PSLs for light emission. This approach, which combines the key advantages of both 1D pillar arrays and 2D graphene sheets, might provide new design opportunities in optoelectronic devices.

Acknowledgment. This work was supported by National Research Foundation of Korea (NRF) through a grant (K207040000307A050000310, Global Research Laboratory (GRL) Program), provided by the Korean Ministry of Education, Science, and Technology (MEST) in 2009.

Supporting Information Available. Additional experimental details, figures, and reference. This material is available free of charge via the Internet at <http://pubs.acs.org>.

REFERENCES AND NOTES

- (1) Park, W. I.; Yi, G.-C. *Adv. Mater.* **2004**, *16*, 87–90.
- (2) Noborisaka, J.; Motohisa, J.; Hara, S.; Fukui, T. *Appl. Phys. Lett.* **2005**, *87*, 093109.
- (3) Thelander, C.; Agarwal, P.; Brongersma, S.; Eymery, J.; Feiner, L. F.; Forchel, A.; Scheffler, M.; Riess, W.; Ohlsson, B. J.; Gösele, U.; Samuelson, L. *Mater. Today* **2006**, *9*, 28–35.
- (4) Tang, Y. B.; Chen, Z. H.; Song, H. S.; Lee, C. S.; Cong, H. T.; Cheng, H. M.; Zhang, W. J.; Bello, I.; Lee, S. T. *Nano Lett.* **2008**, *8*, 4191–4195.
- (5) Garnett, E.; Yang, P. *Nano Lett.* DOI: 10.1021/nl100161z.
- (6) Fan, Z.; Razavi, H.; Do, J.; Moriwaki, A.; Ergen, O.; Chueh, Y.-L.; Leu, P. W.; Ho, J. C.; Takahashi, T.; Reichertz, L. A.; Neale, S.; Yu, K.; Wu, M.; Ager, J. W.; Javey, A. *Nat. Mater.* **2009**, *8*, 648–653.
- (7) Hu, L.; Chen, G. *Nano Lett.* **2007**, *7*, 3249–3252.
- (8) Lee, Y.-J.; Ruby, D. S.; Peters, D. W.; McKenzie, B. B.; Hsu, J. W. P. *Nano Lett.* **2008**, *8*, 1501–1505.
- (9) Cabalu, J. S.; Thomidis, C.; Moustakas, T. D.; Riyopoulos, S.; Zhou, L.; Smith, D. J. *J. Appl. Phys.* **2006**, *99*, No. 064904.
- (10) Keller, S.; Schaake, C.; Fichtenbaum, N. A.; Neufeld, C. J.; Wu, Y.; McGroddy, K.; David, A.; DenBaars, S. P.; Weisbuch, C.; Speck, J. S.; Mishra, U. K. *J. Appl. Phys.* **2006**, *100*, No. 054314.
- (11) Lee, J. M.; Pyun, Y. B.; Yi, J.; Choung, J. W.; Park, W. I. *J. Phys. Chem. C* **2009**, *113*, 19134–19138.
- (12) Nadarajah, A.; Word, R. C.; Meiss, J.; Könenkamp, R. *Nano Lett.* **2008**, *8*, 534–537.
- (13) Park, S. I.; Xiong, Y.; Kim, R. H.; Elvikis, P.; Meitl, M.; Kim, D. H.; Wu, J.; Yoon, J.; Yu, C. J.; Liu, Z.; Huang, Y.; Hwang, K. C.; Ferreira, P.; Li, X.; Choquette, K.; Rogers, J. A. *Science* **2009**, *325*, 977–981.

- (14) Lee, C.-H.; Yoo, J.; Hong, Y. J.; Kim, Y.-J.; Cho, J.; Yi, G.-C.; Jeon, S. R.; Baek, J. H. *Appl. Phys. Lett.* **2009**, *94*, 213101.
- (15) Lee, C.; Wei, X.; Kysar, J. W.; Hone, J. *Science* **2008**, *321*, 385–388.
- (16) Kim, K. S.; Zhao, Y.; Jang, H.; Lee, S. Y.; Kim, J. M.; Kim, K. S.; Ahn, J. H.; Kim, P.; Choi, J. Y.; Hong, B. H. *Nature* **2009**, *457*, 706–710.
- (17) Reina, A.; Jia, X.; Ho, J.; Nezich, D.; Son, H.; Bulovic, V.; Dresselhaus, M. S.; Kong, J. *Nano Lett.* **2009**, *9*, 30–35.
- (18) Unarunotai, S.; Murata, Y.; Chialvo, C. E.; Mason, N.; Petrov, I.; Nuzzo, R. G.; Moore, J. S.; Rogers, J. A. *Adv. Mater.* DOI: 10.1002/adma.200904095.
- (19) Gan, Y. J.; Sun, L. T.; Banhart, F. *Small* **2008**, *4*, 587–591.
- (20) Yi, D. K.; Lee, J. H.; Rogers, J. A.; Paik, U. *Appl. Phys. Lett.* **2009**, *94*, 084104. Kim, M. H.; Choi, J.-Y.; Choi, H. K.; Yoon, S.-M.; Park, O. O.; Yi, D. K.; Choi, S. J.; Shin, H.-J. *Adv. Mater.* **2008**, *20*, 457–461.
- (21) An, S. J.; Chae, J. H.; Yi, G. C.; Park, G. H. *Appl. Phys. Lett.* **2008**, *92*, 121108.
- (22) Kim, J. Y.; Lee, J.; Kim, J.; Kang, B.; Kwon, O. D. *Appl. Phys. Lett.* **2003**, *82*, 25.
- (23) Katz, A.; Abernathy, C. R.; Pearton, S. J. *Appl. Phys. Lett.* **1990**, *56*, 1028.
- (24) Wang, W. H.; Han, W.; Pi, K.; McCreary, K. M.; Miao, F.; Bao, W.; Lau, C. N.; Kawakami, R. K. *Appl. Phys. Lett.* **2008**, *93*, 183107.
- (25) Kong, K.; Choi, Y.; Ryu, B.-H.; Lee, J.-O.; Chang, H. *Mater. Sci. Eng., C* **2006**, *26*, 1207–1210.
- (26) Ni, Z.; Wang, Y.; Yu, T.; Shen, Z. *Nano Res.* **2008**, *1*, 273–291.
- (27) Barros, E. B.; Demir, N. S.; Filho, A. G. S.; Filho, J. M.; Jorio, A.; Dresselhaus, G.; Dresselhaus, M. S. *Phys. Rev. B* **2005**, *71*, 165422.
- (28) Gupta, A.; Chen, G.; Joshi, P.; Tadigadapa, S.; Eklund, P. C. *Nano Lett.* **2006**, *6*, 2667–2673.
- (29) Si, Y.; Samulski, E. T. *Nano Lett.* **2008**, *8*, 1679–1682.
- (30) Green, A. A.; Hersam, M. C. *Nano Lett.* **2009**, *9*, 4031–4036.
- (31) Rich, D. H.; Tang, Y.; Konkar, A.; Chen, P.; Madhukar, A. *J. Appl. Phys.* **1998**, *84*, 6337–6344.
- (32) Li, X.; Cai, W.; An, J.; Kim, S.; Nah, J.; Yang, D.; Piner, R.; Velamakanni, A.; Jung, I.; Tutuc, E.; Banerjee, S. K.; Colombo, L.; Ruoff, R. S. *Science* **2009**, *324*, 1312–1314.